Post-stack velocity analysis by separation and imaging of seismic diffractions[a]

[a]Published in Geophysics, 72, U89-U94, (2007)

Sergey Fomel, Evgeny Landa†, and M. Turhan Taner‡*

ABSTRACT

Small geological features manifest themselves in seismic data in the form of diffracted waves, which are fundamentally different from seismic reflections. Using two field data examples and one synthetic example, we demonstrate the possibility of separating seismic diffractions in the data and imaging them with optimally chosen migration velocities. Our criterion for separating reflection and diffraction events is the smoothness and continuity of local event slopes that correspond to reflection events. For optimal focusing, we develop the local varimax measure. The objectives of this work are velocity analysis implemented in the post-stack domain and high-resolution imaging of small-scale heterogeneities. Our examples demonstrate the effectiveness of the proposed method for high-resolution imaging of such geological features as faults, channels, and salt boundaries.

INTRODUCTION

Diffracted and reflected seismic waves are fundamentally different physical phenomena (Klem-Musatov, 1994). Most seismic data processing is tuned to imaging and enhancing reflected waves, which carry most of the information about subsurface. The value of diffracted waves, however, should not be underestimated (Khaidukov et al., 2004). When seismic exploration focuses on identifying small subsurface features (such as faults, fractures, channels, and rough edges of salt bodies) or small changes in seismic reflectivity (such as those caused by fluid presence or fluid flow during reservoir production), it is diffracted waves that contain the most valuable information.

In this paper, we develop an integrated approach for extracting and imaging of diffracted events. We start with stacked or zero-offset data as input and produce time-migrated images with separated and optimally focused diffracted waves as output. The output of our processing flow can be compared to coherence cubes (Bahorich and Farmer, 1995; Marfurt et al., 1998). While the coherence cube algorithm tries to enhance incoherent features, such as faults, in the migrated image domain, we perform the separation in unmigrated data, where these features appear in the form of diffracted waves.

We also introduce diffraction-event focusing as a criterion for migration velocity analysis, as opposed to the usual "flat-gather" criterion used in seismic imaging. Focusing analysis is applicable not only to multi-coverage prestack data but also to post-stack or single-coverage data.

The idea of extracting information from seismic diffractions is not new. Harlan et al. (1984) used forward modeling and local slant stacks for estimating velocities from diffractions; Landa and Keydar (1998) used common-diffraction-point sections for imaging of diffraction energy and detecting local heterogeneities; Soellner and Yang (2002) simulated diffraction responses for enhancing velocity analysis. Sava et al. (2005) incorporated diffraction imaging in wave-equation migration velocity analysis.

The novelty of our approach is in integration of two essential steps:

1. Separating diffracted and reflected events in the data space,

2. Focusing analysis for automatic detection of migration velocities optimal for imaging diffractions.

We explain both steps and illustrate their application with field and synthetic datasets.

SEPARATING DIFFRACTIONS

The underlying assumption that we employ for separating diffracted and reflected events is that, in a stacked data volume, background reflections correspond to strong coherent events with continuously variable slopes. Removing those events reveals other coherent information, often in the form of seismic diffractions. We propose to identify and remove reflection events with the method of plane-wave destruction (Claerbout, 1992; Fomel, 2002). Plane-wave destruction estimates continuously variable local slopes of dominant seismic events by forming a prediction of each data trace from its neighboring traces with optimally compact non-stationary filters that follow seismic energy along the estimated slopes. Minimizing the prediction residual while constraining the local slopes to vary smoothly provides an optimization objective function analogous to differential semblance (Symes and Carazzone, 1991). Iterative optimization of the objective function generates a field of local slopes. The prediction residual then contains all events, including seismic diffractions, that do not follow the dominant slope pattern. An analogous idea, but with implementation based on prediction-error filters, was previously discussed by Claerbout (1994) and Schwab et al. (1996). Although separation of reflection and diffraction energy can never be exact, our method serves the practical purpose of enhancing the wave response of small subsurface discontinuities.

IMAGING DIFFRACTIONS

How can one detect the spatially-variable velocity necessary for focusing of different diffraction events? A good measure of focusing is the *varimax norm* used by Wiggins (1978) for minimum-entropy deconvolution and by Levy and Oldenburg (1987) for zero-phase correction. The varimax norm is defined as

$$\phi = \frac{N \sum\limits_{i=1}^{N} s_i^4}{\left(\sum\limits_{i=1}^{N} s_i^2\right)^2}\;, \tag{1}$$

where s_i are seismic signal amplitudes inside a window of size N. Varimax is simply related to kurtosis of zero-mean signals.

Rather than working with data windows, we turn focusing into a continuously variable attribute using the technique of *local attributes* (Fomel, 2007a). Noting that the correlation coefficient of two sequences a_i and b_i is defined as

$$c[a,b] = \frac{\sum\limits_{i=1}^{N} a_i\, b_i}{\sqrt{\sum\limits_{i=1}^{N} a_i^2\, \sum\limits_{i=1}^{N} b_i^2}} \tag{2}$$

and the correlation of a_i with a constant is

$$c[a,1] = \frac{\sum\limits_{i=1}^{N} a_i}{\sqrt{N\, \sum\limits_{i=1}^{N} a_i^2}}\;, \tag{3}$$

one can interpret the varimax measure in equation 1 as the inverse of the squared correlation coefficient between s_i^2 and a constant: $\phi = 1/c[s^2,1]^2$. Well-focused signals have low correlation with a constant and correspondingly high varimax.

Going further toward a continuously variable focusing attribute, notice that the squared correlation coefficient can be represented as the product of two quantities $c[s^2,1]^2 = p\,q$, where

$$p = \frac{\sum\limits_{i=1}^{N} s_i^2}{N}\;, \quad q = \frac{\sum\limits_{i=1}^{N} s_i^2}{\sum\limits_{i=1}^{N} s_i^4}\;. \tag{4}$$

Furthermore, p is the solution of the least-squares minimization problem

$$\min_p \sum_{i=1}^{N} \left(s_i^2 - p\right)^2\;, \tag{5}$$

and q is the solution of the least-squares minimization

$$\min_q \sum_{i=1}^{N} \left(1 - q\, s_i^2\right)^2 \ . \tag{6}$$

This allows us to define a continuously variable attribute ϕ_i by using continuously variable quantities p_i and q_i, which are defined as solutions of regularized optimization problems

$$\min_{p_i} \left(\sum_{i=1}^{N} \left(s_i^2 - p_i\right)^2 + R\left[p_i\right]\right) \ , \tag{7}$$

$$\min_{q_i} \left(\sum_{i=1}^{N} \left(1 - q_i\, s_i^2\right)^2 + R\left[q_i\right]\right) \ , \tag{8}$$

where R is a regularization operator designed to avoid trivial solutions by enforcing a desired behavior (such as smoothness). Shaping regularization (Fomel, 2007b) provides a particularly convenient method for enforcing smoothing in an iterative optimization scheme.

We apply the local focusing measure to obtain migration-velocity panels for every point in the image. First, we follow the procedure outlined in the previous section to replace a stacked or zero-offset section with a section containing only separated diffractions. Next, we migrate the data multiple times with different migration velocities. This is accomplished by *velocity continuation* (Fomel, 2003a), a method that performs time-migration velocity analysis by continuing seismic images in velocity with the process also called "image waves" (Hubral et al., 1996). The velocity continuation theory (Fomel, 2003b) shows that one can accomplish time migration with a set of different velocities by making differential steps in velocity similarly to the method of cascaded migrations (Larner and Beasley, 1987) but described and implemented as a continuous process. While comparable in theory to an ensemble of Stolt migrations (Fowler, 1984; Mikulich and Hale, 1992), velocity continuation has the advantage of working directly in the image domain. It is implemented with an efficient and robust algorithm based on the Fast Fourier Transform.

Finally, we compute ϕ_i for every sample point in each of the migrated images. Thus, N in equations 7 and 8 refers to the total number of sample points in an image. The output is *focusing image gathers* (FIGs), exemplified in Figure 1. A FIG is analogous to a conventional migration-velocity analysis panel and suitable for picking migration velocities. The main difference is that the velocity information is obtained from analysis of diffraction focusing as opposed to semblance of flattened image gathers used in prestack analysis.

EXAMPLES

Three different examples illustrate applications of our method to imaging of geological faults and irregular salt boundaries.

Fault detection

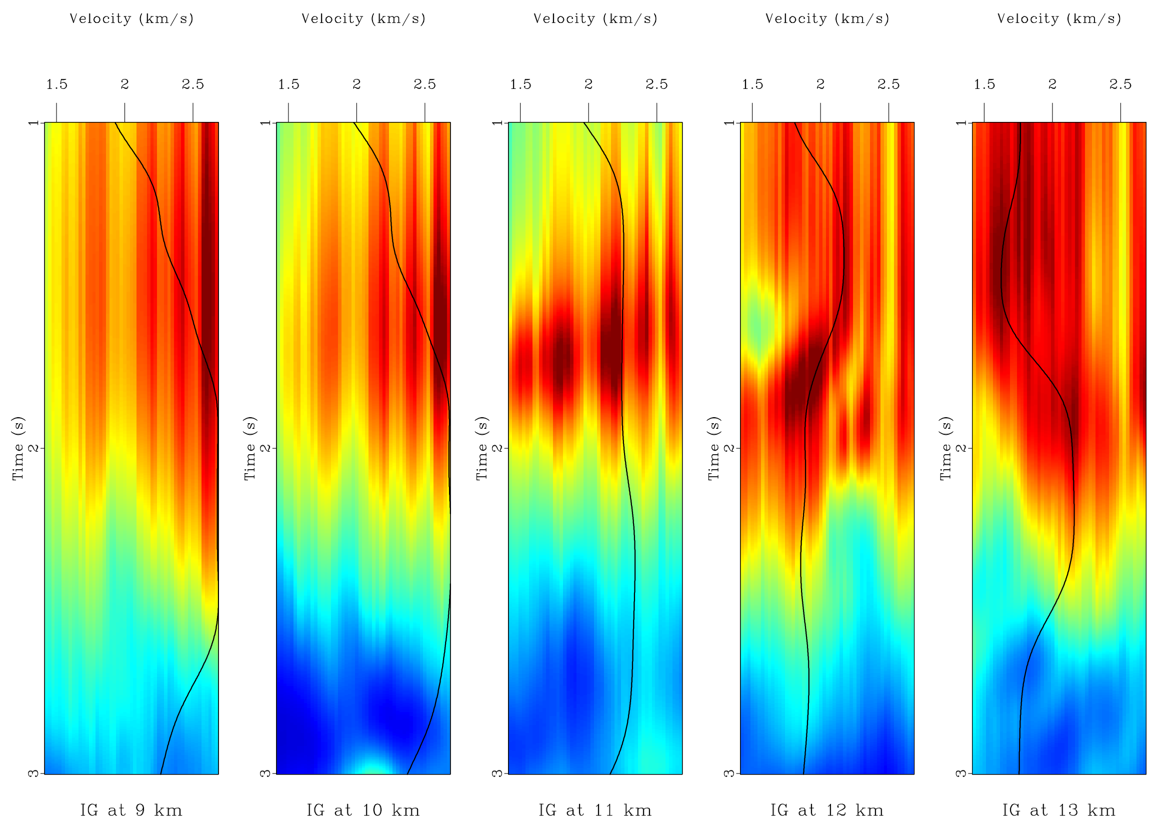

Figure 1: Focusing image gathers (FIG) for post-stack migration velocity analysis by diffraction focusing. Red colors indicate strong focusing. Superimposed black curves are slices of the picked migration velocity shown in Figure 3(b).

The data for our first example are shown in Figure 2(a), which displays a stacked section of a vintage Gulf of Mexico dataset (Claerbout, 2005). Diffractions caused by irregular fault boundaries are preserved in the stack thanks to dip moveout processing but are hardly visible underneath strong reflection responses. Figure 2(b) shows the dominant slope of reflection events estimated by the plane-wave destruction method. Numerous diffractions were separated from reflections by plane-wave destruction and are shown in Figure 3(a).

Figure 3(b) shows the migration velocity picked from focusing common-image gathers (FIGs). Example FIGs are shown in Figure 1. Figure 4(a) is the image of diffracted events, which collapse to collectively form fault surfaces. Figure 4(b) is the image obtained by migrating the original stack with velocities estimated from diffraction focusing analysis. In this final image, fault surfaces align with discontinuities in seismic reflectors. The image compares favorably with images of the same dataset from the conventional processing shown by Claerbout (2005).

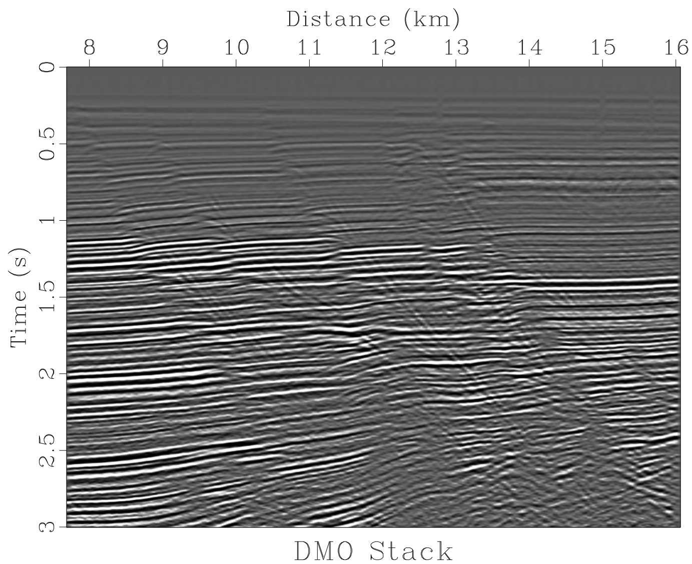

(a)

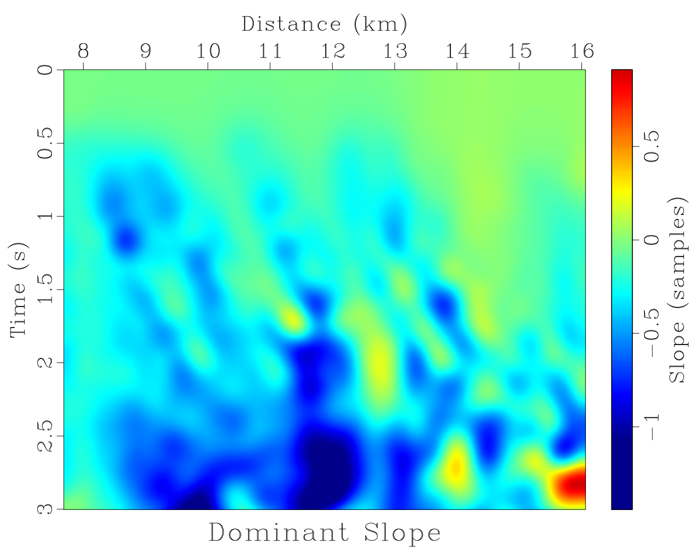

(b)

Figure 2: First test example. (a) Stacked section from a Gulf of Mexico dataset. (b) Local slopes estimated by plane-wave destruction.

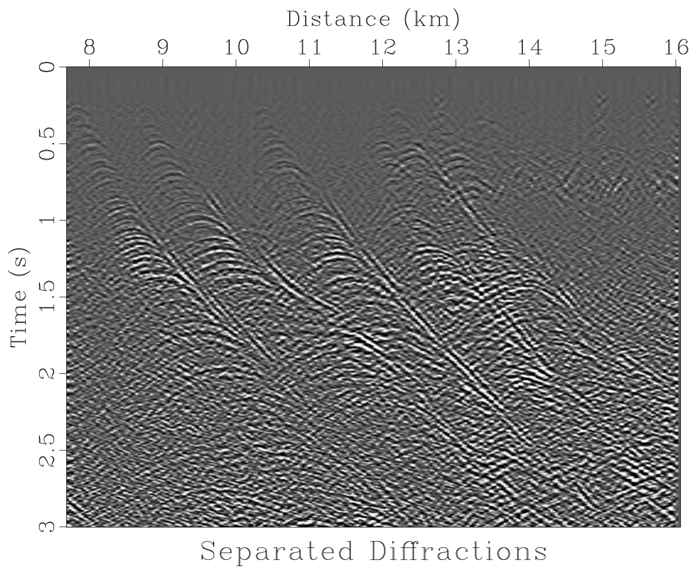

(a)

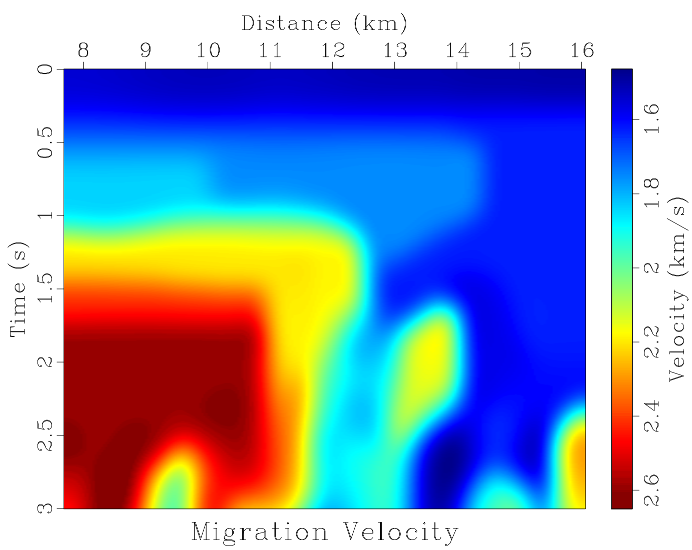

(b)

Figure 3: Diffraction separation. (a) Diffraction events separated from data in Figure 2(a). (b) Migration velocity picked from local varimax scans after velocity continuation of diffractions.

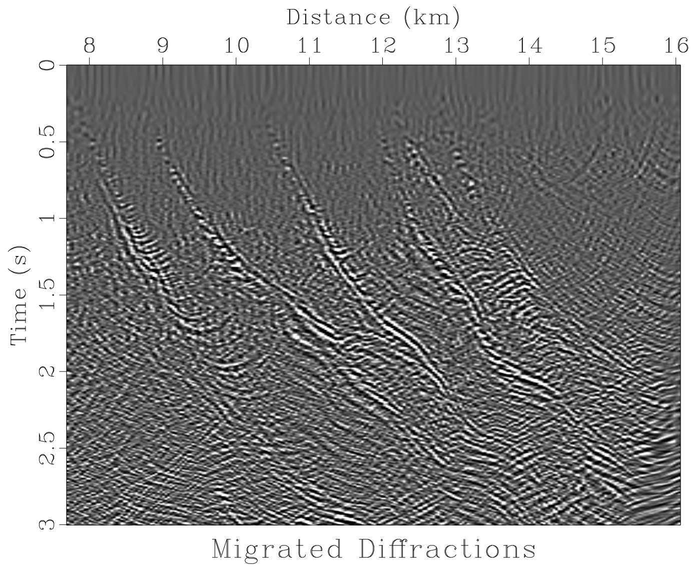

(a)

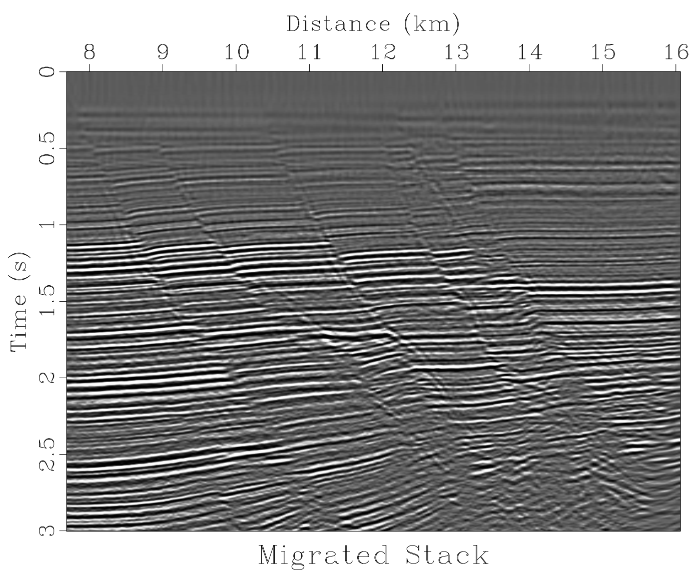

(b)

Figure 4: Migrated images. (a) Migrated diffractions from Figure 3(a). (b) Initial data from Figure 2(a) migrated with velocity estimated by diffraction imaging.

Salt detection

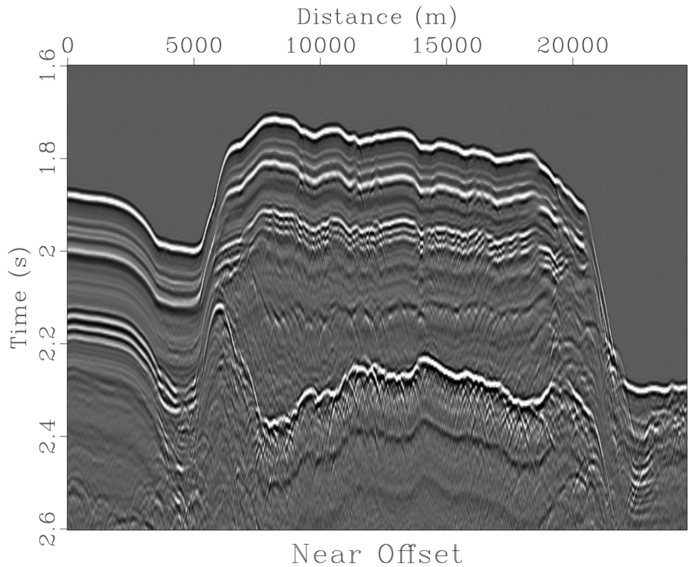

(a)

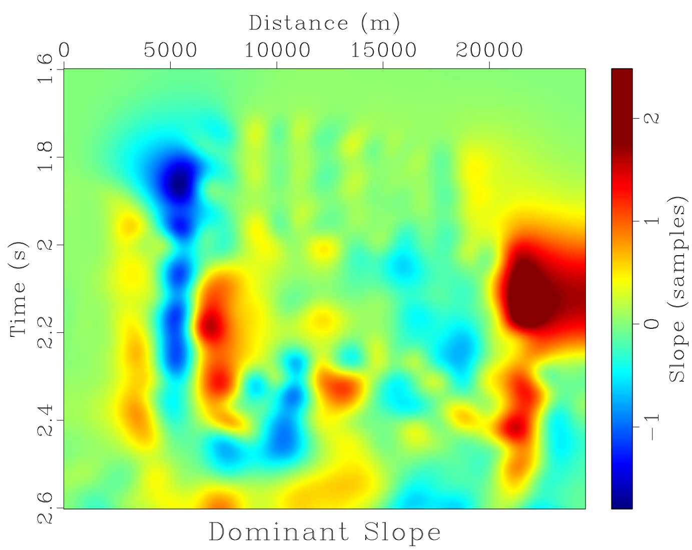

(b)

Figure 5: Second test example. (a) Near-offset section from a Gulf of Mexico dataset. (b) Local slopes estimated by plane-wave destruction.

Figure 5(a) shows another example, also from the Gulf of Mexico. We used the nearest-offset section for diffraction analysis. Plane-wave destruction estimates dominant slopes of continuous reflection events [Figure 5(b)] and reveals numerous diffractions generated by rough edges of a salt body [Figure 6(a)]. We used shaping regularization (Fomel, 2007b) with the smoothing radius of 40-by-10 samples to constrain the slope-estimation process. Focusing analysis generates a time migration velocity [Figure 6(b)] suitable for collapsing diffractions [Figure 7(a)]. Both sharp edges of the

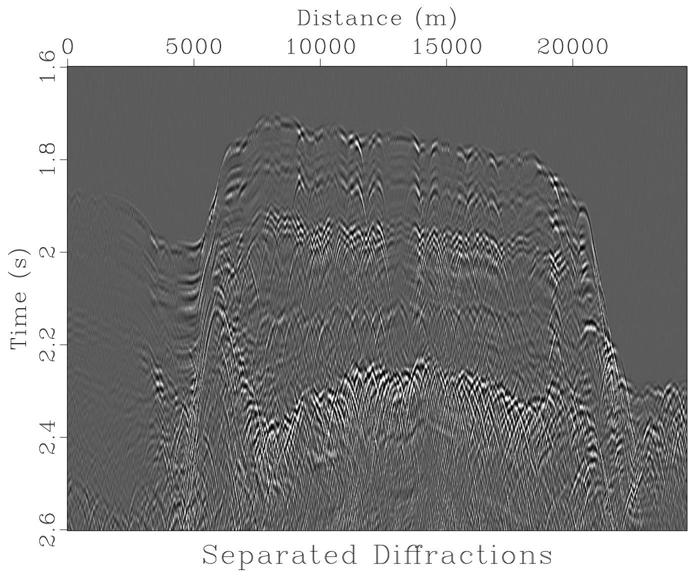

(a)

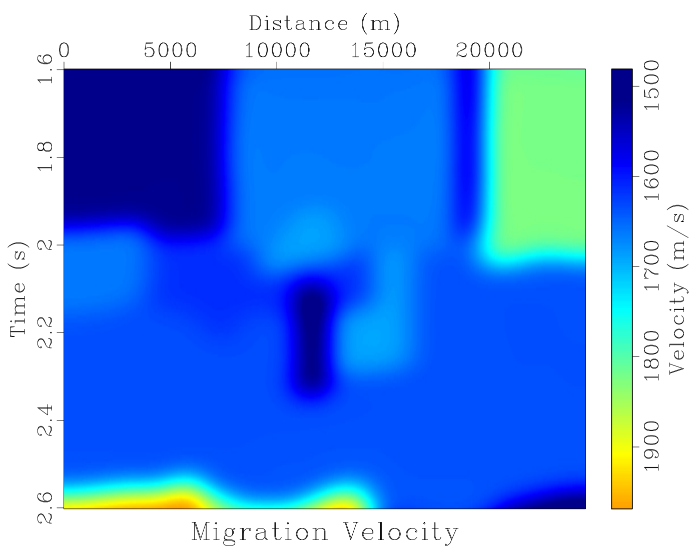

(b)

Figure 6: Diffraction separation. (a) Diffraction events separated from data in Figure 5(a). (b) Migration velocity picked from local varimax scans after velocity continuation of diffractions.

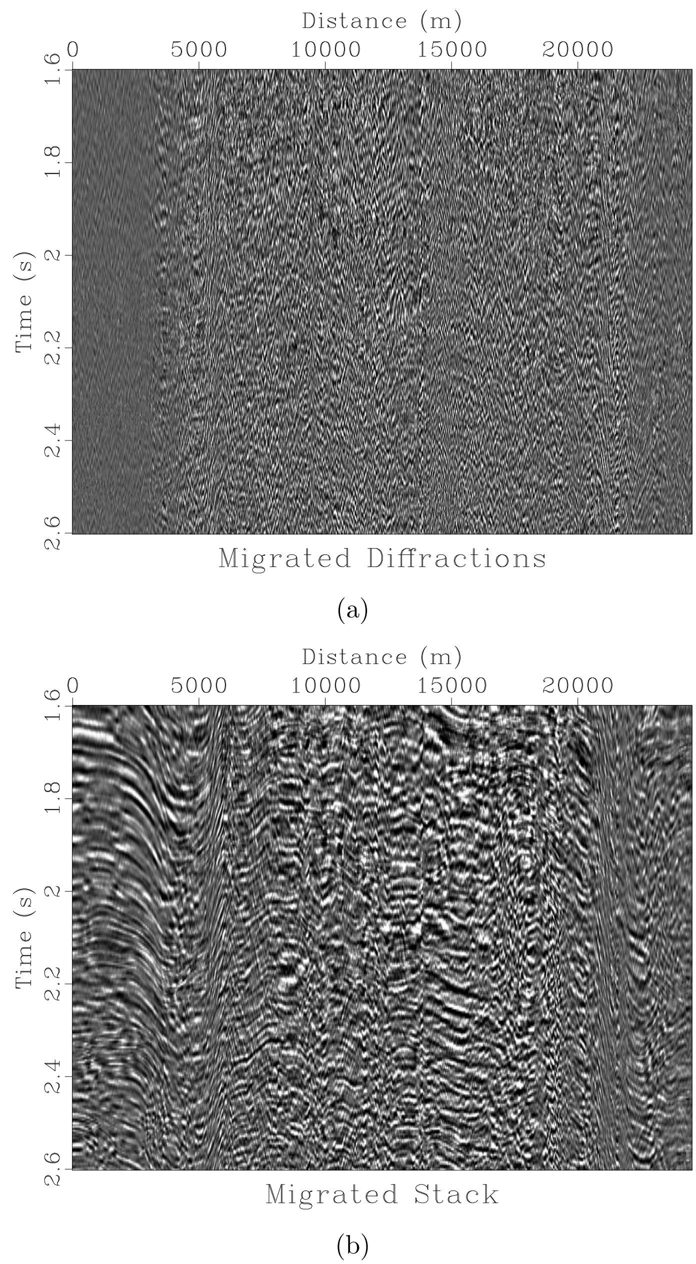

Figure 7: Migrated images. (a) Migrated diffractions from Figure 6(a). (b) Initial data from Figure 5(a) migrated with velocity estimated by diffraction imaging.

salt body and continuous specular reflections appear in the final image [Figure 7(b)]. Inevitably, prestack depth migration (as opposed to time migration) is required to properly position the salt boundary in depth. Time migration, however, provides a reasonable first-order approximation computed at a small fraction of the cost.

Channel detection

The third example is a 3-D synthetic dataset. The velocity model was designed to simulate a complex sand channel geometry in a deep-water clastic reservoir (Figure 8(a)). Including an overburden with stochastically generated velocity fluctuations on top of the reservoir model, we generated zero-offset data shown in Figure 8(b). The data contain reflections from continuous parts of the model and numerous diffractions generated by the channel edges. Separating diffractions using in-line plane-wave destruction (Figure 9), we compare depth-migrated images of the original data and of the separated diffractions (Figure 10). The fine details of the stacked channel geometry are revealed by diffraction imaging.

CONCLUSIONS

We have developed a method of efficient migration velocity analysis based on separation and imaging of seismic diffractions. The efficiency follows from the fact that the proposed analysis is applied in the post-stack domain as opposed to the conventional prestack velocity analysis. We used continuity of dominant reflections in the zero-offset or stacked sections as a criterion for separating reflections from diffractions. We then imaged separated diffractions using local focusing analysis for picking optimal migration velocities. A prestack extension of our approach was presented by Taner et al. (2006).

ACKNOWLEDGMENTS

We thank TOTAL for partially supporting this work. The field datasets used in this study were released by Western Geophysical, and the synthetic reservoir model was created by Jim Jennings at the Bureau of Economic Geology in collaboration with Chevron. We are grateful to Ken Larner for a thorough and helpful review.

REFERENCES

Bahorich, M., and S. Farmer, 1995, 3-D seismic discontinuity for faults and stratigraphic features: The coherence cube: The Leading Edge, **14**, 1053–1058. (Discussion with reply by author in TLE-15-3-172).

Claerbout, J. F., 1992, Earth Soundings Analysis: Processing Versus Inversion: Blackwell Scientific Publications.

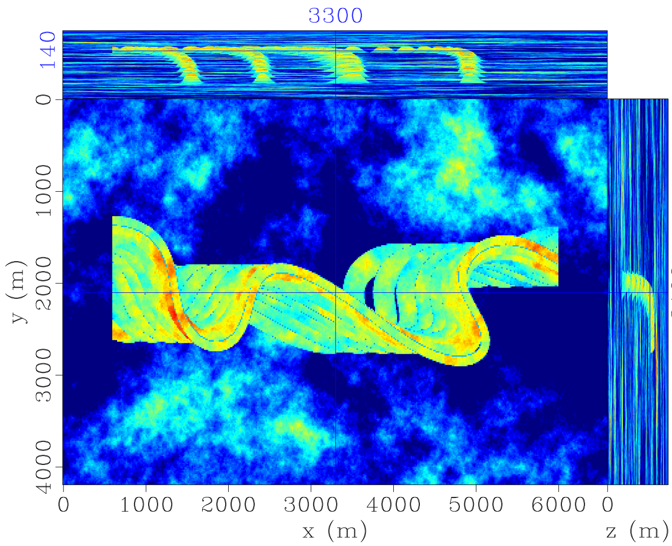

(a)

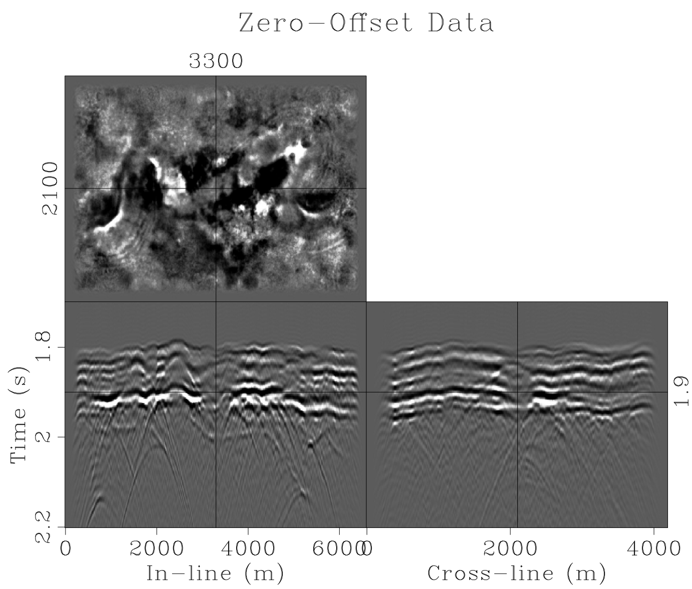

(b)

Figure 8: 3-D synthetic test. (a) Synthetic velocity model for a channelized reservoir. (b) Modeled zero-offset data.

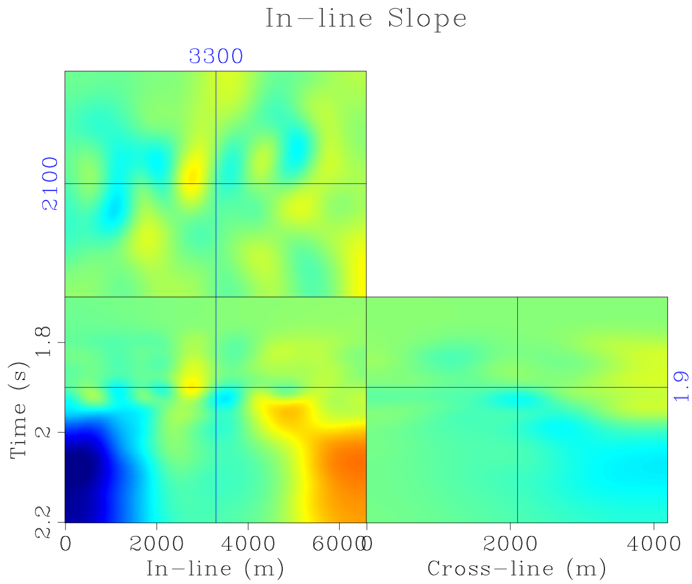

(a)

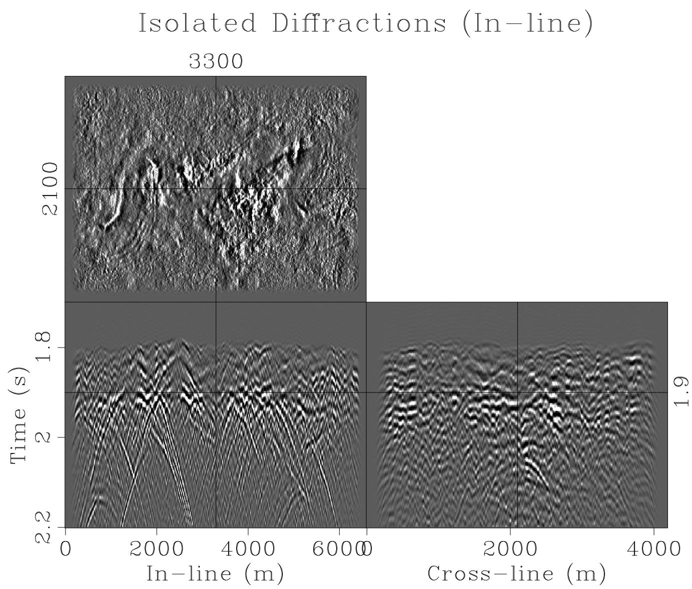

(b)

Figure 9: Diffraction separation for the 3-D synthetic test from Figure 8. (a) Dominant in-line slope estimated by plane-wave destruction. (b) Diffractions separated from the data.

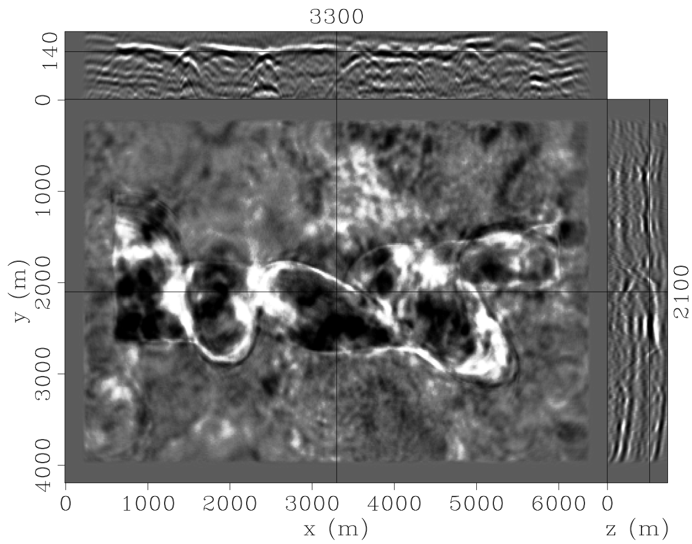

(a)

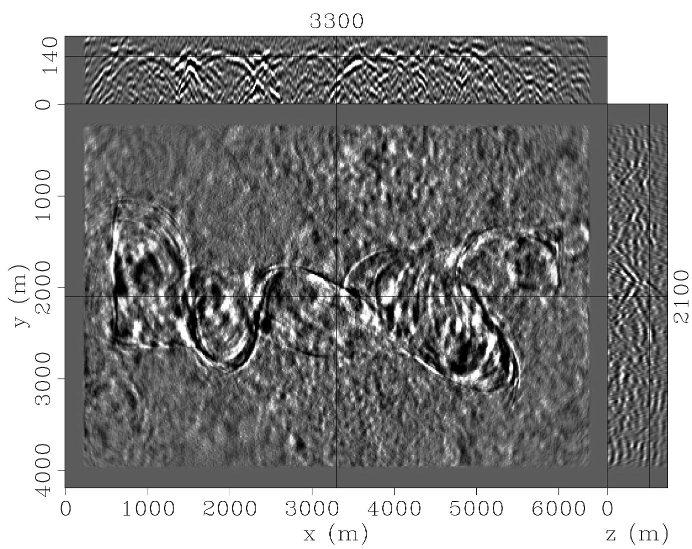

(b)

Figure 10: Depth migration of the 3-D synthetic test data. (a) Migrated data. (b) Migrated diffractions.

———, 1994, Applications of two- and three-dimensional filtering: 64th Ann. Internat. Mtg, Soc. of Expl. Geophys., 1572–1575.

———, 2005, Basic Earth Imaging: Stanford Exploration Project.

Fomel, S., 2002, Applications of plane-wave destruction filters: Geophysics, **67**, 1946–1960.

———, 2003a, Time-migration velocity analysis by velocity continuation: Geophysics, **68**, 1662–1672.

———, 2003b, Velocity continuation and the anatomy of residual prestack time migration: Geophysics, **68**, 1650–1661.

———, 2007a, Local seismic attributes: Geophysics, **72**, A29–A33.

———, 2007b, Shaping regularization in geophysical-estimation problems: Geophysics, **72**, R29–R36.

Fowler, P., 1984, Velocity independent imaging of seismic reflectors: 54th Ann. Internat. Mtg, Soc. of Expl. Geophys., Session:S1.8.

Harlan, W. S., J. F. Claerbout, and F. Rocca, 1984, Signal/noise separation and velocity estimation: Geophysics, **49**, 1869–1880.

Hubral, P., M. Tygel, and J. Schleicher, 1996, Seismic image waves: Geophysical Journal International, **125**, 431–442.

Khaidukov, V., E. Landa, and T. Moser, 2004, Diffraction imaging by focusing-defocusing: An outlook on seismic superresolution: Geophysics, **69**, 1478–1490.

Klem-Musatov, K., 1994, Theory of Seismic Diffractions: Soc. of Expl. Geophys. (Edited by Hron F. Fronta and Larry Lines).

Landa, E., and S. Keydar, 1998, Seismic monitoring of diffraction images for detection of local heterogeneities: Geophysics, **63**, 1093–1100.

Larner, K., and C. Beasley, 1987, Cascaded migrations - Improving the accuracy of finite-difference migration: Geophysics, **52**, 618–643. (Errata in GEO-52-8-1165).

Levy, S., and D. W. Oldenburg, 1987, Automatic phase correction of common-midpoint stacked data: Geophysics, **52**, 51–59.

Marfurt, K. J., R. L. Kirlin, S. L. Farmer, and M. S. Bahorich, 1998, 3-D seismic attributes using a semblance-based coherency algorithm: Geophysics, **63**, 1150–1165.

Mikulich, W., and D. Hale, 1992, Steep-dip v(z) imaging from an ensemble of Stolt-like migrations: Geophysics, **57**, 51–59.

Sava, P. C., B. Biondi, and J. Etgen, 2005, Wave-equation migration velocity analysis by focusing diffractions and reflections: Geophysics, **70**, U19–U27.

Schwab, M., J. Claerbout, and C. Holden, 1996, Revealing geological discontinuities by plane reflector suppression: 66th Ann. Internat. Mtg, Soc. of Expl. Geophys., 302–305.

Soellner, W., and W. Yang, 2002, Diffraction response simulation: A 3D velocity inversion tool: 72nd Ann. Internat. Mtg, Soc. of Expl. Geophys., 2293–2296.

Symes, W. W., and J. J. Carazzone, 1991, Velocity inversion by differential semblance optimization: Geophysics, **56**, 654–663.

Taner, M. T., S. Fomel, and E. Landa, 2006, Prestack separation of seismic diffractions using plane-wave decomposition: 76th Ann. Internat. Mtg, Soc. of Expl. Geophys., 2401–2404.

Wiggins, R., 1978, Minimum entropy deconvolution: Geoexploration, **16**, 21–25.